THE ASTROPHYSICAL JOURNAL, 423:237–247, 1994 March 1

ANISOTROPIC HIGH-EXCITATION EMISSION AND CHEMICAL ABUNDANCES IN THE SEYFERT 2 GALAXY NGC 5643

HENRIQUE R. SCHMITT[1] AND THAISA STORCHI-BERGMANN[2]
Departamento de Astronomia, IF-UFRGS, CP 15051, CEP 91501-970, Porto Alegre, RS, Brazil
AND
JACK A. BALDWIN
Cerro Tololo Inter-American Observatory, National Optical Astronomy Observatories, Casilla 603, La Serena, Chile
Received 1993 May 18; accepted 1993 September 3

ABSTRACT

We present narrow-band images in the lines [O III] λ5007 and Hα + [N II] λλ6548, 6584 and long-slit spectroscopy along the bar of the Seyfert 2 galaxy NGC 5643. The continuum subtracted [O III] and Hα images show that the emission of the high excitation gas is elongated along the bar direction and extends to ≈1 kpc to each side of the nucleus. Farther out, there is low-excitation emission due to H II regions along the bar. Our data confirm previous suggestions of a biconical morphology for the high-excitation gas and indicate that the cone axis is slightly tilted relative to the bar.

We study the reddening in the central regions and find that the most obscured region is located at ≈3″ W from the peak of the continuum, which is also the region with the highest gas density. We speculate that the active nucleus is hidden and located there. The available data is consistent with the nuclear obscuration being due to the presence of a dusty torus, which would also be responsible for collimating the ionizing radiation and producing the biconical morphology.

The stellar population derived from the spectra is moderately old in the central region and young in the H II regions along the bar. Within 10″ of the nucleus we find that the absorption lines are diluted by a blue continuum. We discuss the origin of this continuum.

The fluxes of the emission lines are obtained and plots showing the distribution of the line fluxes and ratios along the bar are constructed. The ionic and total abundances of the H II regions are calculated. The oxygen and nitrogen abundances increase toward the center reaching, respectively, solar and 2 times solar values. Photoionization model calculations for the high-excitation extended narrow-line region gas confirm these values and indicate that the sulphur has the same abundance relative to solar as nitrogen.

Subject headings: galaxies: abundances — galaxies: individual (NGC 5643) — galaxies: Seyfert — galaxies: stellar content — galaxies: structure

1. INTRODUCTION

Recent investigations have been finding an increasing number of Seyfert 2 galaxies with optical morphologies in the emission lines that indicate anisotropic escape of the ionizing radiation (Wilson 1992 and references therein; Storchi-Bergmann, Wilson, & Baldwin 1992; Pogge 1988a, b; Storchi-Bergmann & Bonatto 1991). For at least eight galaxies with available narrow-band images and long-slit spectroscopy it was verified that the data are consistent with the presence of an obscuring torus which collimates the ionizing radiation (Storchi-Bergmann, Mulchaey, & Wilson 1991, hereafter SBMW), as predicted in the "Unified Scheme" for Seyfert galaxies (Pier & Krolik 1992; Antonucci 1993 and references therein).

NGC 5643 is a southern barred spiral galaxy, with morphological type SBc(s)II–III and a high-excitation emission-line spectrum (Sandage 1978), classified as a low-luminosity Seyfert 2 by Phillips, Charles, & Baldwin (1983). NGC 5643 seems to be another example in which we have an obscured active nucleus with anisotropic escape of the ionizing radiation: in observations with an imaging Fabry-Perot spectrometer, Morris et al. (1985) found that this galaxy presents extended optical line emission, with an elongated morphology along the E-W direction (which is coincident with the bar direction). A similar structure is seen in radio observations with the VLA, and a model is proposed in which a gaseous disc perpendicular to the bar collimates the radio emission and causes anisotropic escape of the ionizing continuum along the bar. In order to further investigate the properties of the active nucleus and high-excitation gas of NGC 5643 we have obtained narrow-band images of the nuclear regions, and long-slit spectroscopy along the bar of the galaxy.

Another goal of this work is to study the chemical abundance of the nuclear gas in order to verify previous results that indicate a selective enrichment of nitrogen and sulphur in active nuclei (Storchi-Bergmann & Pastoriza 1989, 1990). These results were based on emission-line ratios from the narrow line region (NLR), which were compared with photoionization model results. As NGC 5643 has several H II regions just beyond the high-excitation gas, we will be able to compare the chemical abundances obtained for these regions (for which the physical processes are better understood) with those derived for the NLR.

Another property of NGC 5643 is that it is an X-ray source with $L_{X(0.2-4\mathrm{KeV})} = 1.32 \times 10^{41}$ ergs s^{-1} as found from *ROSAT* observations by Boller et al. (1992). Antonucci & Olszewski (1985) derived a bolometric flux of 2.1×10^{-9} ergs

[1] CNPq fellow.
[2] Visiting Astronomer at the Cerro Tololo Inter-american Observatory, operated by the Association of Universities for Research in Astronomy, Inc., under contract with the National Science Foundation.

cm^{-2} s^{-1}. NGC 5643 is also an *IRAS* source with coadded *IRAS* flux $F_{IR} = 1.915 \times 10^{-9}$ ergs cm^{-2} s^{-1} (Mulchaey et al. 1993) and infrared spectral indexes $\alpha(60, 25) = -1.96$ and $\alpha(100, 60) = -1.71$. Phillips et al. (1983) found from radio observations $P_{6cm} = 8 \times 10^{19}$ W Hz^{-1} sr^{-1}.

We adopt the systemic velocity obtained by Reif et al. (1982): 1200 km s^{-1} (heliocentric) or 970 km s^{-1} (galactocentric). Using $H_0 = 75$ km s^{-1} Mpc^{-1}, the distance of the galaxy is then 13 Mpc, and the angular scale is 1″ = 62.7 pc.

2. OBSERVATIONS

2.1. *Direct Imaging*

Direct images of NGC 5643 through filters centered on the redshifted [O III] λ5007 and Hα + [N II] λλ6548, 6584 emission lines (which we will refer to from now on as [O III] image and Hα image), as well as on the adjacent continua, were obtained at the Cerro Tololo Inter-American Observatory (CTIO) 0.91 m telescope using a CCD detector on the night of 1990 March 12/13. The scale of the frames is 0.″5 per pixel. Table 1 presents a log of the observations.

The individual images were corrected for bias, flat-fielded, and flux-calibrated using a standard star from Stone & Baldwin (1983). The point-spread function (PSF) of the line plus continuum and the continuum images were compared, and the one with the smaller PSF was convolved with a Gaussian function in order to match the one with the larger PSF. Each continuum image was then scaled by a factor such that the integrated number of counts for the stars in the field was equal to the corresponding value in the line plus continuum frame. Finally, images in [O III] and Hα were produced by subtracting the appropriate continuum frame from the line plus continuum frame.

2.2. *Long-Slit Spectroscopy*

A long-slit spectrum of NGC 5643 at position angle 90° (which lies approximately along the bar of the galaxy) was obtained with a CCD detector on the Ritchey-Chrétien spectrograph attached to the CTIO 4 m telescope on the night of 1992 May 28/29. The exposure time was 30 minutes. The observations covered the spectral range 3400 Å–7500 Å at 8 Å resolution. The slit width was 2″, and the scale along the spatial direction was 0.″9 per pixel. The reductions, including flux calibrations, followed standard IRAF procedures.

Spectra were extracted binning together 2 pixels at the nucleus and to 18″ E and W of the nucleus, each corresponding to a 2.″0 × 1.″8 angular aperture (113 × 125.5 pc at the galaxy). Farther out, more pixels were binned together in order to improve the signal-to-noise (S/N) ratio. Table 2 presents the positions relative to the nucleus of the extractions as well as the corresponding window dimensions.

TABLE 1

CCD IMAGES OF NGC 5643

Filter (Å/ΔÅ)	Exposure (minutes)	Comments
4700/190	15	continuum
5024/15	25	[O III] λ5007
6477/72	10	continuum
6606/76	10	Hα + [N II] λλ6548, 6584

TABLE 2

POSITIONS AND WINDOWS FOR THE EXTRACTED SPECTRA

Position	Window
Nucleus, 1.″8 E, 1.″8 W, 3.″6 E, 3.″6 W, ..., 18.″0 E, 18.″0 W	1.″8
27.″9 W	18.0
46.8 W	19.8
65.7 W	18.0
78.3 W	7.2
19.8 E	1.8
25.2 E	9.0
33.3 E	7.2
43.2 E	12.6
55.8 E	12.6
67.5 E	10.8
81.0 E	16.2

3. RESULTS

3.1. *Morphology*

Figure 1 shows the Hα image (before subtraction of the continuum) of NGC 5643. In this image one can see the nuclear region and the bar running E-W, as well as several H II regions along the bar and spiral arms.

The continuum-subtracted [O III] calibrated image is shown in Figure 2. This image maps the high-excitation gas, which is restricted to the nuclear region, shown enlarged in the figure. It can be seen that the gas distribution presents an elongated morphology aligned with the bar, with dimensions at the 2 σ isophotal level of 30″(1.9 kpc) along the E-W direction and 13.″5 (850 pc) along the N-S direction. We will call this region the extended narrow-line region (hereafter ENLR). The point of strongest emission is coincident with the nucleus (as determined from the continuum frames), but there is a second (fainter) peak of emission at about 6″ to the E. The emission to the W extends to similar distance from the nucleus as that to the E, although is much fainter.

Figure 3 shows the Hα continuum-subtracted calibrated image, corresponding to the same region shown in Figure 2. It can be seen that its morphology is similar to that of the [O III] image, except for a blob at a distance of 16″ E (1 kpc) from the nucleus, which is not present in the [O III] image and is thus an H II region.

We have then constructed an excitation map, shown in Figure 4, dividing the [O III] image by the Hα image. The inner isophotes are consistent with a projected conical morphology for the high-excitation gas. The point with highest [O III]/Hα ratio is not coincident with the nucleus but is located at 5.″6 E (350 pc), suggesting that the excitation is highest at this location. A similar behavior of the excitation was found in the ionization cone of NGC 3281 (Storchi-Bergmann, et al. 1992). To the W of the nucleus [O III]/Hα decreases, but presents a small increase again at 8.″3 W (520 pc). Although the [O III]/Hα ratio essentially maps the excitation, it is also affected by reddening. We will come back to this point in § 3.3.

3.2. *Stellar Population*

After correcting the extracted spectra for the galactic reddening $E(B-V)_g = 0.125$ (Burstein & Heiles 1984), we have measured the ratio between the continuum fluxes at 5870 Å and 4020 Å. We have also measured the equivalent widths (W_λ) of the following absorption features: K(Ca II) (spectral window 3908 Å–3952 Å), G band (4284 Å–4318 Å) and Mg I (5156 Å–5196 Å) (caution should be taken in the use of this line in the

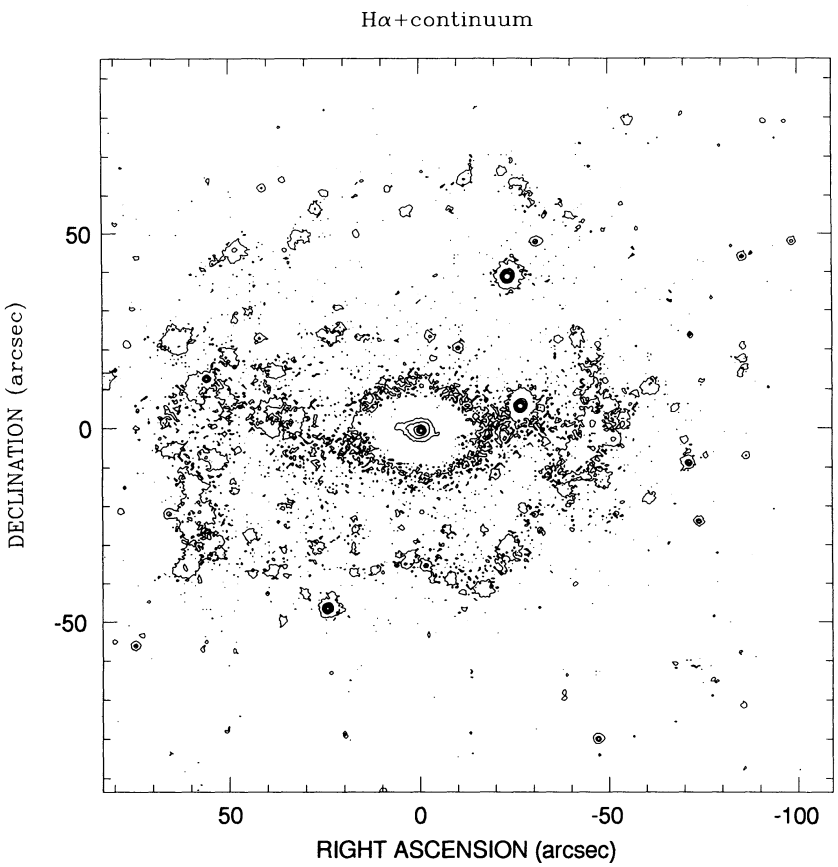

FIG. 1.—Contour map of the Hα (line plus continuum) image of NGC 5643; contours are at 4%, 7%, 10%, 18%, 35%, 51%, and 67% of the peak brightness above the sky. N is to the top and E to the left.

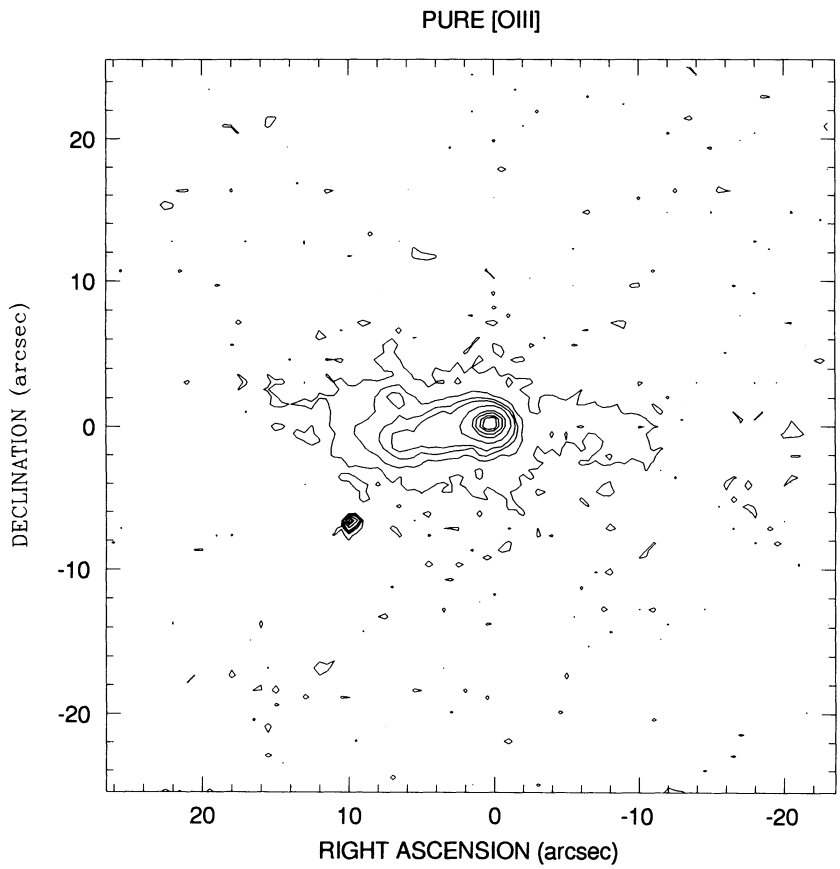

FIG. 2.—Contour map of the continuum subtracted [O III] λ5007 image of the central region; contours are at 1%, 3%, 6%, 9%, 17%, 35%, 49%, 67%, and 80% of the peak brightness above the sky.

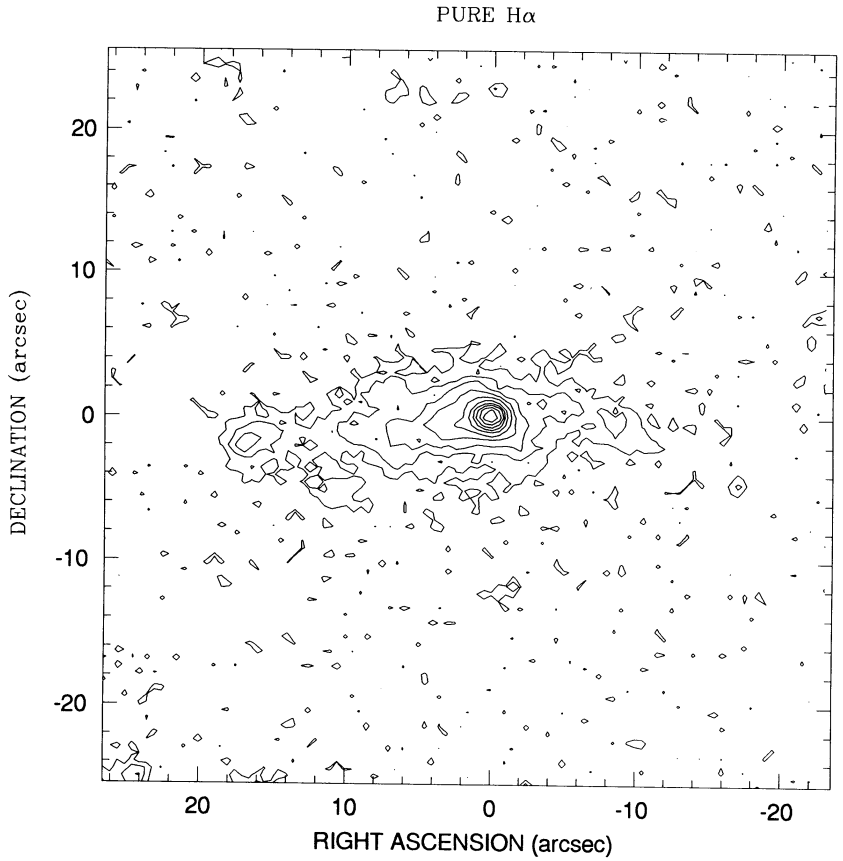

FIG. 3.—Contour map of the continuum subtracted Hα + [N II] λλ6548, 6584 image of the central region; contours are at 1%, 2%, 4%, 7%, 12%, 20%, 40%, 54%, and 74% of the peak brightness above the sky.

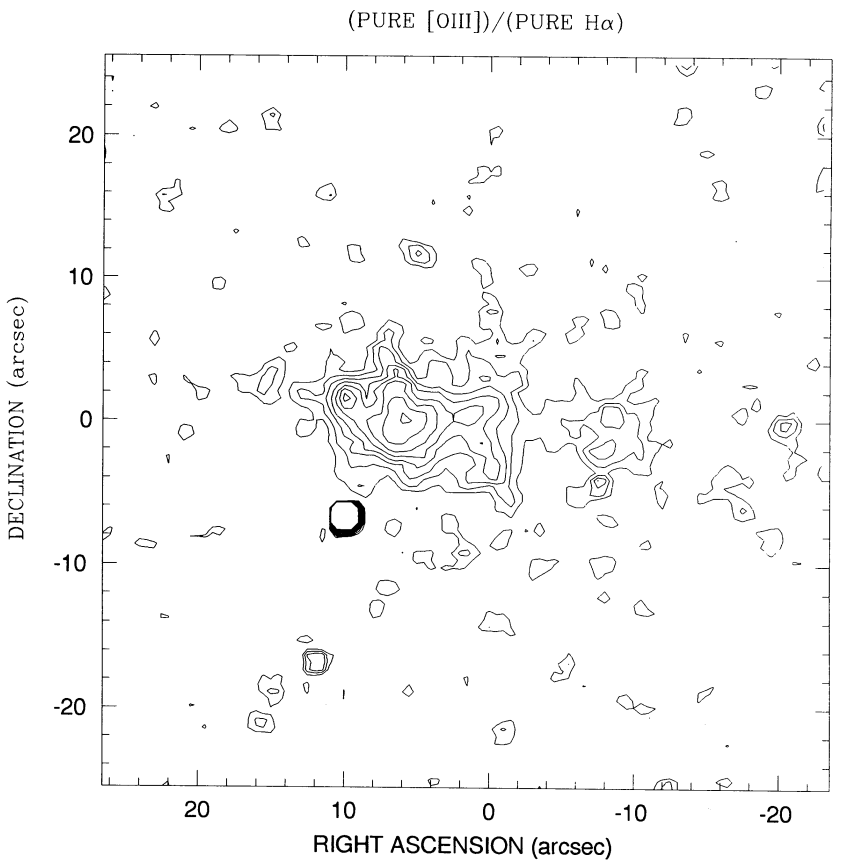

FIG. 4.—"Excitation map" of the nuclear region, the result of dividing the [O III] λ5007 map by the Hα + [N II] λλ6548, 6584 map

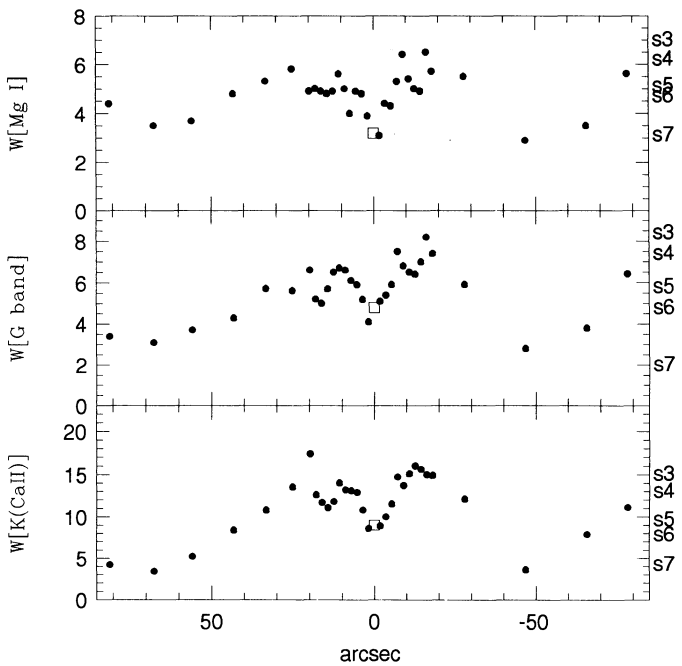

FIG. 5.—W_λ's are plotted as a function of distance from the nucleus. The nucleus is represented by a square. Characteristic W_λ values for the templates S3, S4, S5, S6, and S7 are shown at the right edge of each panel.

nuclear region due to contamination by [N I] λ5200 emission), in order to study the stellar population along the bar.

Figure 5 shows W_λ as a function of distance from the nucleus for the various absorption lines. As a reference, we also show at the right edge of each figure typical values corresponding to stellar population templates for spiral galaxies, from the library of synthetic spectra of Bica (1988). The templates with W_λ values similar to the ones observed by us are S3, S4, S5, S6, and S7. These templates are synthetic spectra composed of different percentages of star cluster spectra of several ages and metallicities. The template S3 contains only the contribution of stars older than 10^9 yr; in S4 95% of the light at 5870 Å comes from old stars and 5% from young and intermediate age ones; in S5 the contribution is 85% from old stars and 15% from young and intermediate age; in S6 the old star contribution is 75%, and 25% is from young and intermediate age ones; finally, in S7 30% corresponds to old stars and 70% to young and intermediate age ones.

It can be seen that the largest W_λ values are found between 10″ and 20″ to either side of the nucleus, corresponding to S3–S4 templates. The W_λ values systematically drop by 30%–50% right at the nucleus and fall off even more at positions far from it, corresponding then to S6–S7 templates.

Figures 6 shows the continuum ratio 5870 Å/4020 Å for the same positions as above. It can be seen that they are consistent with the W_λ's at these locations, corresponding to the same population template, except for the nucleus, where the ratios imply redder populations than the W_λ's or the presence of interstellar reddening.

3.3. *Emission Lines*

We show in Figure 7 the spectrum of the nucleus (which samples the high excitation emission) and of an H II region at

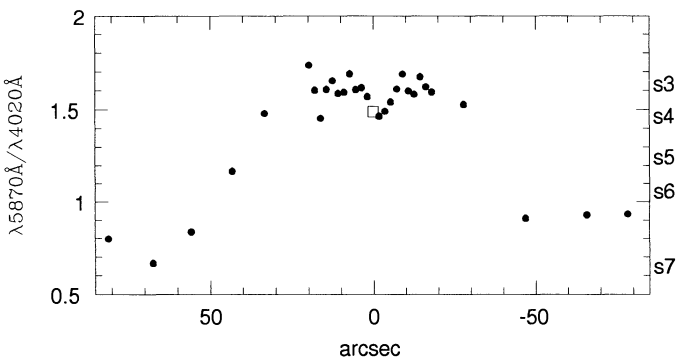

FIG. 6.—Continuum ratio 5870 Å/4020 Å as a function of distance from the nucleus. Values of the templates are shown at the right edge of the figure.

43″.2 E. The fluxes of the emission lines were measured in order to study the gas excitation, reddening, density and abundances at several locations along the bar. As the spectral resolution of the stellar population templates is much lower than that of our spectra, we preferred not to subtract the templates from the spectra. We only corrected the Hα and Hβ emission lines (the more affected) for the effect of the underlying absorption using the corresponding equivalent widths in the stellar population templates. The values of the measured fluxes relative to the Hβ flux are shown in Table 3. We identify, in the last column, the region from which each spectrum originates.

We will use through the rest of this paper the following notation: [O III] to represent [O III] $\lambda\lambda$4959 + 5007, [N II] for [N II] $\lambda\lambda$6548 + 6584, [S II] for [S II] $\lambda\lambda$6717 + 6731 and [O II] for [O II] λ3727.

In Figure 8 we plot the logarithm of the fluxes of the emission lines [O III], Hα, [O II], [N II] as a function of distance from the nucleus. It can be seen that the strongest [O III] emission comes from the ENLR, while for the lower excitation lines there is relatively strong emission also from the H II regions along the bar. In Figure 9 we plot the fluxes of [O I]

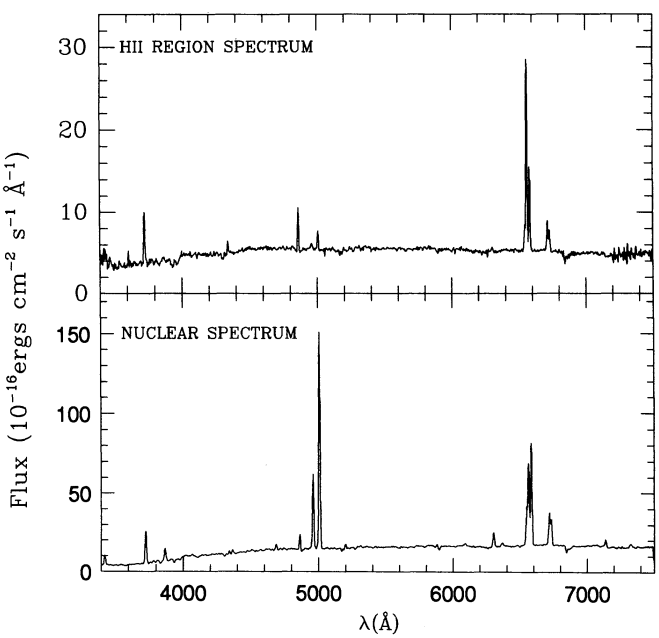

FIG. 7.—Spectrum of the nucleus (*bottom*) and of an H II region 43″.2 E (*top*).

TABLE 3

EMISSION LINE FLUXES RELATIVE TO Hβ

Position	Wavelength (Å) [Ne v] 3426	[O ii] 3727	[Ne iii] 3869	[O iii] 4363	He ii 4686	[O iii] 5007	[N i] 5200	[O i] 6300	Hα 6563	[N ii] 6584	[S ii] 6717	[S ii] 6731	[Ar iii] 7135	F(Hβ)	Observation
Nucleus	0.87	3.06	1.20	0.42	0.32	13.51	0.32	1.00	5.81	6.33	2.08	1.64	0.37	114.0	a
1.″8 W	1.26	3.81	1.37	0.30	0.31	14.52	0.31	1.08	6.40	6.89	2.20	2.00	0.91	56.9	a
3.6 W	...	3.22	1.06	0.49	0.26	12.21	...	1.35	7.18	8.65	3.09	2.79	0.44	16.3	a
5.4 W	...	2.87	...	...	0.33	10.39	...	0.96	6.19	7.50	2.75	2.25	...	10.2	a
7.2 W	...	2.90	0.97	...	...	11.78	...	0.73	6.10	7.27	2.53	1.95	...	7.9	a
9 W	...	2.39	...	...	...	12.00	...	0.70	5.89	7.13	2.73	1.84	...	7.0	a
10.8 W	...	1.54	...	...	...	7.73	0.75	4.56	5.33	2.04	1.40	...	...	5.2	a
12.6 W	...	1.13	...	...	...	4.32	...	...	3.11	3.97	1.50	0.84	...	3.8	a
14.4 W	...	1.75	...	...	...	3.54	...	...	3.17	3.50	...	...	...	2.4	a
16.2 W	...	...	...	...	...	3.88	...	...	3.19	3.44	...	...	...	1.6	a
18 W	...	...	...	...	...	4.00	...	...	3.10	4.30	...	...	...	1.0	a
1.8 E	0.79	4.10	1.32	0.46	0.34	13.39	0.30	0.97	5.50	5.99	2.10	1.80	0.45	87.3	a
3.6 E	0.73	4.17	1.19	0.34	0.35	13.69	0.26	0.78	4.38	4.92	1.79	1.41	0.39	61.6	a
5.4 E	0.72	3.54	1.07	0.23	0.32	12.28	0.17	0.57	3.60	3.70	1.30	1.02	0.34	50.5	a
7.2 E	0.87	4.42	1.30	0.33	0.30	11.81	0.14	0.53	3.56	3.30	1.09	0.84	0.29	38.2	a
9 E	0.91	3.94	1.19	0.35	0.28	9.78	0.13	0.48	3.58	2.82	0.98	0.67	...	27.9	a
10.8 E	0.86	3.39	1.05	0.19	0.26	7.23	...	0.31	3.83	2.51	0.84	0.64	...	19.1	a–b
12.6 E	...	2.46	0.66	...	...	4.60	...	0.33	4.23	2.44	0.84	0.67	...	14.4	a–b
14.4 E	...	1.53	0.30	...	...	2.20	...	0.16	4.89	2.52	0.81	0.62	...	15.9	a–b
16.2 E	...	1.37	...	...	...	1.24	...	...	4.96	2.35	0.72	0.51	...	16.4	a–b
18 E	...	1.56	...	...	...	1.05	...	...	4.49	2.26	0.69	0.51	...	9.4	a–b
19.8 E	...	2.39	...	...	...	1.33	...	...	5.08	2.97	0.89	0.78	...	3.6	a–b
27.9 W	...	1.65	...	...	...	...	...	...	3.10	3.06	1.14	0.89	...	8.0	c
46.8 W	...	1.22	...	...	...	0.23	...	0.08	4.06	1.72	0.59	0.42	...	139.0	b
65.7 W	...	1.56	...	...	...	...	...	...	3.10	1.58	0.69	0.53	...	16.3	c
78.3 W	...	1.66	...	...	...	...	...	...	3.13	1.57	0.68	0.45	...	4.7	c
25.2 E	...	1.10	...	...	...	1.41	...	...	3.10	2.41	0.78	0.63	...	9.7	c
33.3 E	...	1.07	...	...	...	0.58	...	...	4.43	2.03	0.55	0.41	...	31.6	b
43.2 E	...	1.18	...	...	...	0.38	...	...	4.44	1.88	0.72	0.50	...	55.9	b
55.8 E	...	1.45	...	...	...	...	...	...	4.12	1.69	0.79	0.61	...	26.7	c
67.5 E	...	1.66	...	...	...	0.40	...	...	3.81	1.52	0.82	0.53	...	39.6	b
81 E	...	2.33	...	...	...	0.62	...	...	3.86	1.31	0.76	0.48	...	27.2	b

NOTES.—Hβ flux is in 10^{-14} ergs cm^{-2} s^{-1}. In the last column, a refers to ENLR, b to H II region, and c to the bar of galaxy.

λ6300 and the high-excitation emission lines [Ne v] λ3426, [Ne iii] λ3869 and He ii λ4686, which can only be found in the inner region of the ENLR. It can be seen that the emission is more extended to the E side of the nucleus, falling off abruptly to the W. The high-ionization line [Fe vii] λ6087 was found in the nucleus and in the spectra at 1.″8 E and 1.″8 W.

The gas excitation can be further studied using the emission line ratios [O iii]/Hβ and [O iii]/[O ii], which are good ionization parameter indicators. These ratios are shown in Figure 10. [O iii]/[O ii] was corrected for reddening using the ratio Hα/Hβ (see below), assuming an intrinsic recombination value of 3.1. It can be seen that these ratios are high throughout all the ENLR, falling more or less abruptly at its edges.

The [N ii]/Hα and [S ii]/Hα ratios are also a measure of the gas excitation, although they are also sensitive to the presence of shocks and to the abundance of the gas (we will come back to this point in the next section). These ratios are also shown in Figure 10. The [N ii]/Hα ratio has a value between 1.4 and 1.8 for the points between 20″ W and 3.″6 E from the nucleus, then decreases gradually to the east, reaching the lowest value of 0.6. The ratio [S ii]/Hα shows similar behavior, being about 0.8 between 20″ W and 3.″6 E, decreasing out gradually to 0.25.

The [S ii] λ6717/λ6731 ratio, corresponding gas density, Hα/Hβ, and corresponding $E(B-V)$ are shown in Figure 11. It can be seen that the highest density values (≈ 450 cm^{-3}) do not correspond to the nucleus, but to 1.″8 W and 3.″6 W. The

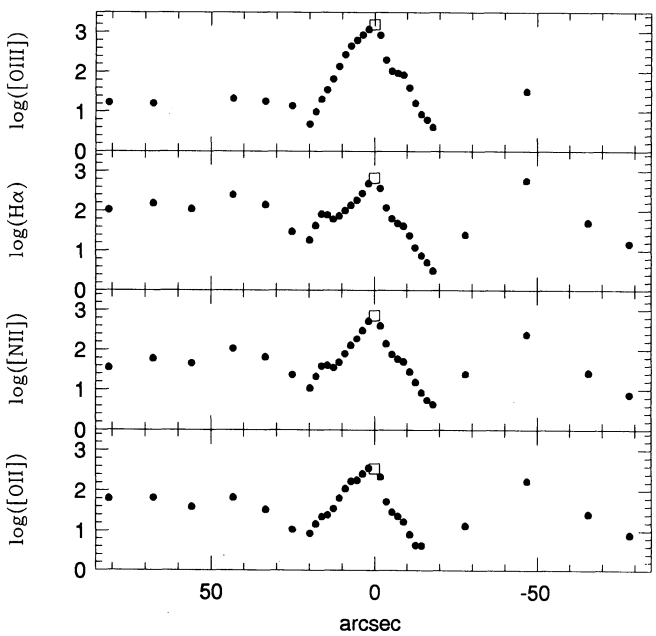

FIG. 8.—Logarithm of emission-line fluxes as a function of distance from the nucleus, in units of 10^{-16} ergs cm^{-2} s^{-1}.

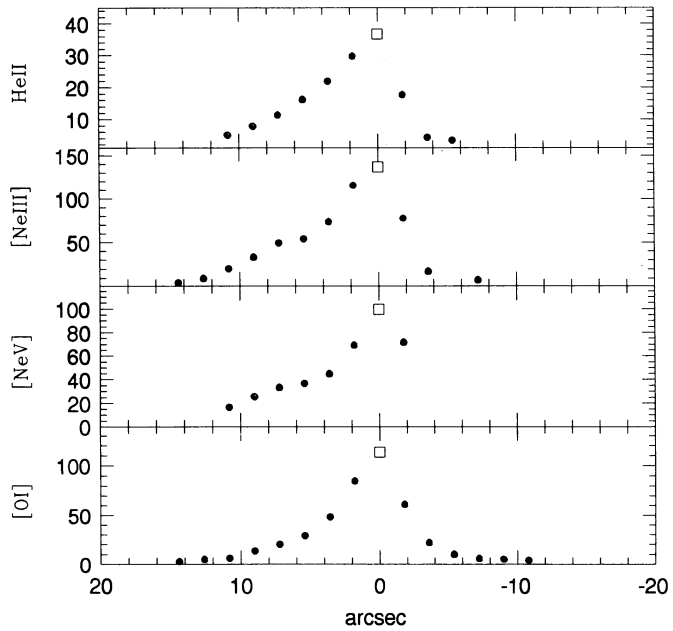

FIG. 9.—Emission-line fluxes as a function of distance from the nucleus, in units of 10^{-16} ergs cm^{-2} s^{-1}.

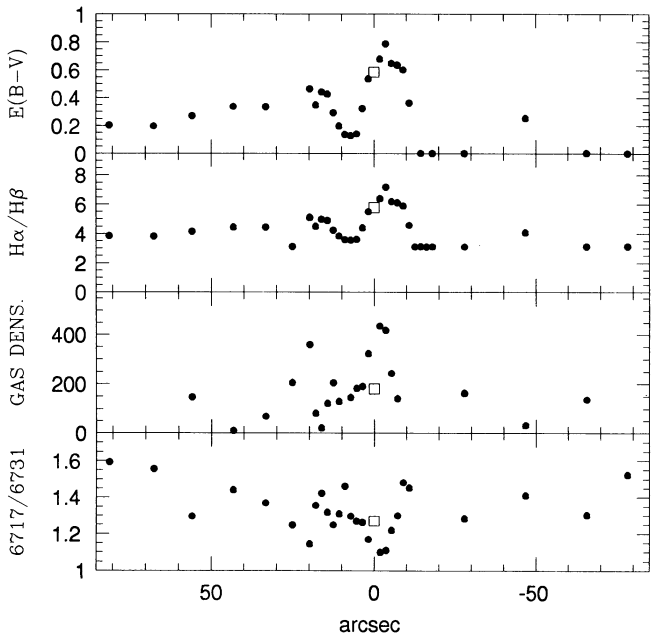

FIG. 11.—From bottom to top: emission-line ratio [S II] λ6717/[S II] λ6731; gas density in cm^{-3}; emission line ratio Hα/Hβ; calculated reddening $E(B-V)$ for intrinsic Hα/Hβ = 3.1.

density at the nucleus is about 200 cm^{-3}. Several points along the ENLR present densities of this order or smaller. Inspection of the $E(B-V)$ plot shows that the points with the highest density are also the ones with the highest reddening, with $E(B-V) = 0.70$–0.80. At the nucleus $E(B-V) = 0.60$, while to the E, there is an abrupt decrease to $E(B-V) = 0.15$ at 5″, and farther out a small increase again to $E(B-V) = 0.2$–0.25.

We have also calculated the ratio [O III]/(Hα + [N II]), in order to compare with the excitation map (Fig. 4). In Figure 12 we show both the observed values and the ones corrected for reddening. The observed ratio shows the same behavior as in the excitation map, but when it is corrected for reddening, the whole region from about 9″ E to 9″ W presents similarly high values, indicating high excitation in all the ENLR. The smaller [O III]/(Hα + [N II]) value at the nucleus and to the W of the nucleus is thus a reddening effect.

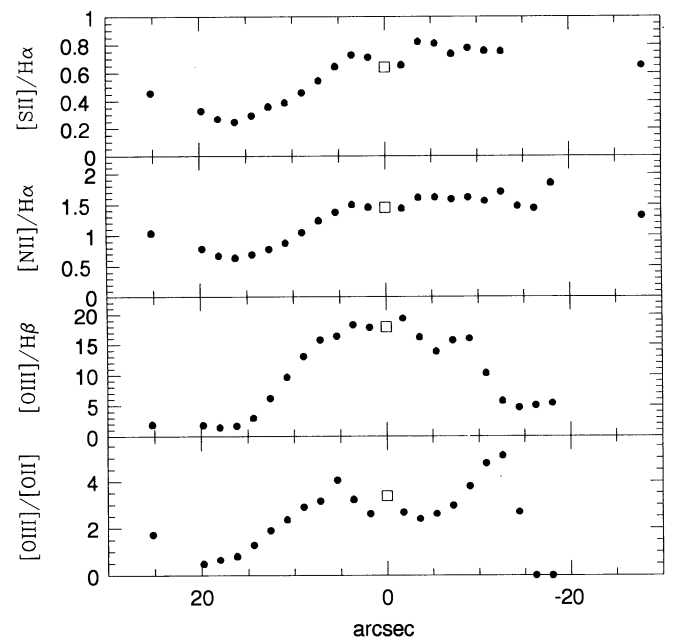

FIG. 10.—Emission-line ratios along the ENLR. [O III]/[O II] was corrected for reddening.

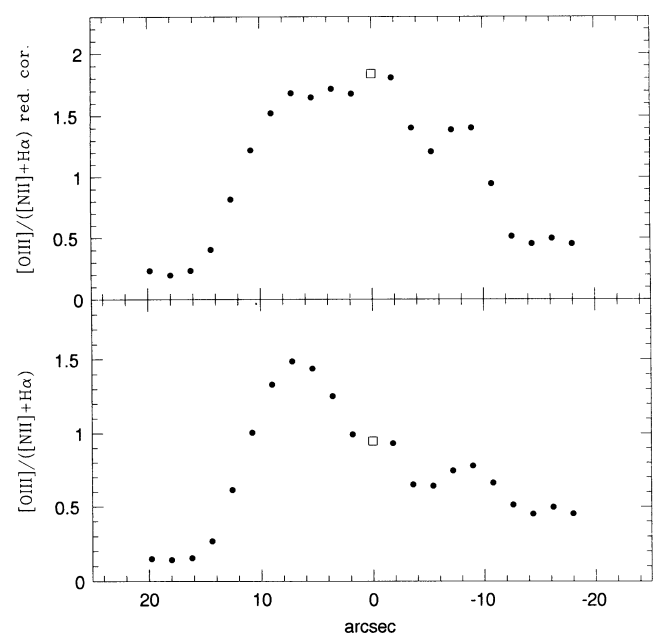

FIG. 12.—Emission-line ratio [O III]/(Hα + [N II]) in the ENLR: (*bottom*) observed; (*top*) corrected for reddening.

4. DISCUSSION

4.1. *Stellar Population, Reddening, and Excitation*

The W_λ's and continuum ratio 5870 Å/4020 Å (Figs. 5 and 6) indicate that the stellar population between 10″ and 20″ at both sides of the nucleus is dominated by old and intermediate age components. Farther out, the continuum becomes bluer and W_λ decreases, consistently indicating the increasing contribution of young stars in the H II regions beyond the ENLR.

In the nucleus the situation is different: the continuum has the same color as in the parts just outside the nucleus (i.e., still quite red, indicating an S3 population), but the W_λ values decrease to values characteristic of about an S6 population. We interpret these contradictory results to be due to dilution of the stellar continuum by a featureless active galactic nucleus (AGN) continuum which has been reddened and scattered throughout the immediate volume around the actual continuum source. From Figure 10 it can be seen that the reddening is indeed high at the nucleus and neighboring points.

Farther out in the ENLR the reddening seems to have a different effect on the continuum and in the gas emission: while the continuum ratio remains constant at the expected value for an S3–S4 template, suggesting no or little reddening, the gas emission indicates a strong reddening to the W and small reddening to the E. The strong reddening to the W can explain the more abrupt decrease in this direction of the blue high excitation emission lines along the ENLR shown in Figure 9. The line ratio [O III]/Hβ and the reddening corrected ratios [O III]/[O II] and [O III]/(Hα + [N II]) (Figs. 10 and 12) show that the excitation of the gas to the W is the same as that to the E. Our interpretation is that we are seeing two similar elongated structures of high-excitation gas, one in front of the bar to the E and the other behind the bar to the W, with the latter being obscured by dust in the bar.

Morris et al. (1985) propose a model in which the gas flows down the bar toward the nucleus, forming a disc orthogonal to the bar major axis. This disc could then collimate the radio emission (as they observe) and also the ionizing continuum that would escape within a cone along the major axis of the bar. Our results suggest that the disc axis must be tilted relative to the bar, such that the ionizing continuum illuminates gas in front of the bar to the E and behind the bar to the W.

It is interesting to point out that Morris et al. (1985) find that the region of greatest line width and blueshift (-100 km s^{-1} relative to predicted velocities from the derived rotation curve) is located at about 3″ W of the peak continuum brightness and speculate that there could be the Seyfert nucleus. From Figure 11 it can be seen that we find the strongest reddening and highest gas density at this same position, corroborating the suggestion that the Seyfert nucleus could be located there.

4.2. *Obscuration of the Nucleus*

If the nucleus is indeed hidden at $\approx$3″ W of the peak brightness, then the observed dilution of the W_λ values at the central points would not be due to direct contribution of the blue ionizing continuum, but probably to its scattered light. We can test if we are seeing the ionizing continuum directly by assuming a spectral shape and using the observed blue continuum flux to estimate the number of ionizing photons coming in our direction. We can then compare this number with the number of ionizing photons seen by the gas in the ENLR; if the source radiates isotropically and the nucleus is not obscured, the two numbers should be the same. This method is described by Wilson (1992) and was used by Kinney et al. (1991) and Storchi-Bergmann et al. (1992).

We have adopted the spectral shape for the ionizing source $F_\nu = A\nu^{-1.5}$. From the dilution of W(K [Ca II]) λ3934 Å at the nucleus, and assuming that the stellar population value is that corresponding to the region between 10″ and 20″ from the nucleus, we obtain a flux for the blue continuum at 3934 Å of 5.3×10^{-16} ergs cm^{-2} s^{-1} Å^{-1}. After correcting for the nuclear reddening of $E(B-V) = 0.6$, we get for the number of ionizing photons at Earth $N_{\rm ion} = 0.362$ photons cm^{-2} s^{-1}.

We have then used the photoionization code CLOUDY (Ferland 1991) to obtain the ionization parameter, U, from the emission-line ratios along the ENLR. From the ionization parameter we can calculate the number of ionizing photons emitted by the nuclear continuum source per second. When scaled to the distance of the Earth, the flux of these ionizing photons is

$$N_{\rm ph} = Unr^2c/R^2 \text{ photons cm}^{-2}\text{ s}^{-1},$$

where n is the gas density, r is the distance from the ionizing source of the point where the emission lines are measured, and R is the distance of the galaxy. This calculation gives $N_{\rm ph} =$ 7.69 photons cm^{-2} s^{-1}.

Comparing the number of ionizing photons seen by the gas with the number of ionizing photons seen at Earth gives the result $N_{\rm ph}/N_{\rm ion} \approx 21$. We thus conclude that if the nucleus is an isotropic UV source and if the dilution we observe in the W_λ at the nucleus is due to direct nuclear continuum light, it is further absorbed by $\approx$3 mag. Another possibility is that the nucleus is much more obscured (and not located at the position corresponding to the peak of the continuum light) and that the observed dilution in the central W_λ's is due to scattered nuclear continuum light. This possibility is supported by the fact that the dilution is observed not only at the nucleus, but also in the neighboring points. A diffuse excess in the near-UV continuum emission, interpreted as scattered nuclear continuum light, was recently observed by Pogge & De Robertis (1993) in an imaging study of three Seyfert 2 galaxies with ionization cones.

4.3. *Origin of the Mid- and Far-Infrared Emission*

From the above discussion, as well as from the results of Morris et al. (1985), we conclude that this galaxy is another example in which we have a conical morphology probably resulting from shadowing by a dusty obscuring torus. We follow the reasoning of SBMW in order to test this hypothesis: using the observed opening angle of the cone, as well as the photon flux seen by the high excitation gas, we can calculate the luminosity incident on the torus L_P; if the torus is indeed present, this luminosity should be reemitted in the infrared, and L_P should be comparable to $L_{\rm IR}$ obtained from the *IRAS* fluxes (after correction for contribution from the disk of the galaxy).

The necessary parameters for the calculations are 1) the photon flux in the direction of the cone, which was calculated in the previous section, 2) the opening angle of the bicone, which we adopt $\theta = 50°$ as estimated from Figure 4 and 3) the fraction of the IR luminosity which is emitted by the nucleus. We have used the scale factor 0.36, given by Roche et al. (1991) as the ratio between the 12 μm luminosity as observed from the ground (with a small aperture) and the corresponding *IRAS* luminosity. A similar method was applied by Edelson & Malkan (1986) to a sample of Seyfert 1 and 2 galaxies: they

have used ground-based measurements in small apertures at 10.6 μm and 21 μm to calculate the fraction of the *IRAS* fluxes at 12 μm and 25 μm due to nuclear emission. The fractions at 12 μm agreed with those at 25 μm. The same scale factor was used to calculate the nuclear emission at 60 μm and 100 μm. As Edelson & Malkan (1986) say, this probably overestimates the nuclear contribution at these wavelengths, as the bulk of emission could arise in the disk. On the other hand, for a few galaxies for which they had ground-based small aperture fluxes also at 100 μm, the scale factors are essentially the same as those for 12 μm. We thus adopt the same scale factor for all *IRAS* wavelengths, keeping in mind that the calculated L_{IR} may be an upper limit.

The calculations give a predicted torus luminosity of $L_P = 7 \pm 5 \times 10^9\ L_\odot$. For the observed nuclear infrared luminosity we get L_{IR} (nuclear) $\leq 3.6 \times 10^9\ L_\odot$. These values fit well into the trend found by SBMW (see their Fig. 1) for the other galaxies with ionization cones and suggest that a dusty torus is indeed present.

4.4. *Chemical Abundance*

4.4.1. H II *Regions*

We calculated the ionic abundances of O^+, O^{++}, S^+, and N^+ for the H II regions, using a three-level atom calculation (McCall 1984). A two-zone model was adopted for the electron temperature: for O^{++} we used T([O III]) obtained from the calibration of Pagel et al. (1979), as it was not possible to measure the emission-line [O III] λ4363 in our spectra; for O^+, N^+, and S^+ we used T([O II]) from the parameterization given by Campbell, Terlevich, & Melnick (1986). For the gas density we used the value calculated from the ratio [S II] λ6717/λ6731. From the ionic abundances, the total abundances relative to the solar value were calculated, using the following assumptions: $O/H = O^+/H^+ + O^{++}/H^+$ and $N/O = N^+/O^+$. Although Garnett (1990) has recently pointed out that the last relation should be used with caution for high-metallicity H II regions, we have compared our results with Garnett's Figure 2 and concluded that the maximum error introduced by this assumption in the nitrogen abundance is 20%. We have not calculated the total abundance of sulphur, owing to the absence of information about the abundance of S^{++} (Garnett 1989). The adopted solar abundance values were N = 7.08, O = 8.91, and S = 7.23 from Aller (1987) and Grevesse (1984).

The results of the calculations are given in Table 4. From the errors in the measurement of the emission-line fluxes and the uncertainty in the determination of the temperature, we estimate that the mean errors in the calculation of the abundances are about 0.2 dex for the H II region at 81″ E and about 0.1 dex for the remaining ones. In Figure 13 we plot the total abundances of N and O as a function of distance from the nucleus, where a clear gradient is observed: 12 + log (O/H) increases from 8.62 (0.5 times the solar value) at 81″ from the nucleus to 8.84 (0.9 times solar) at 33″; 12 + log (N/H) increases from 7.66 to 8.16 (0.5 to 1.5 times solar). Drawing a straight line through the points (we preferred to fit a line by eye due to the small number of points of our sample; see e.g., Vila-Costas & Edmunds 1992) and giving less weight to the point corresponding to the H II region at 81″ E owing to its larger uncertainty, we get the slopes -3.1×10^{-3} dex arsec^{-1} (-0.05 dex kpc^{-1}) for oxygen and -6.6×10^{-3} dex arsec^{-1} (-0.11 dex kpc^{-1}) for nitrogen. Although based on a small number of data points, these gradients are well within the range presented by the oxygen abundance in similar Sc galaxies (Vila-Costas & Edmunds 1992). It can be seen that N/H shows a steeper gradient than O/H. We also show in Figure 14 that there is a linear dependence between log (N/O) and 12 + log (O/H). This kind of behavior is expected if nitrogen is at least in part a secondary element, which means that its production depends on the initial CNO abundance of the stars producing it. We have compared our result with the models of chemical evolution presented by Alloin et al. (1979) in their Figure 4. The locii occupied by our points agree very well with the results of the models in which nitrogen is partially primary and partially secondary.

We have compared our calculated oxygen abundance with that obtained from the parameterization of Dopita & Evans (1986) and also with the recent calibration of McGaugh (1991). In both cases the abundances show a similar gradient to that obtained from our calculations, but with a systematic shift of 0.15 and 0.2 dex, respectively, towards higher abundances. As

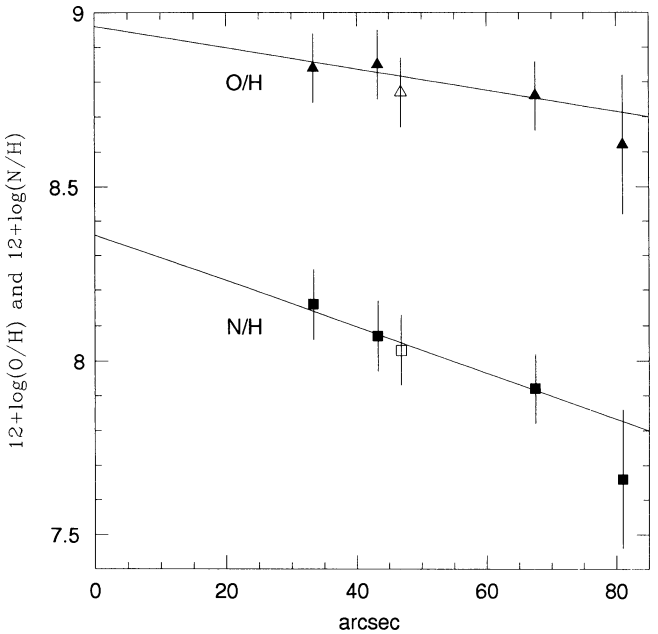

FIG. 13.—Nitrogen and oxygen abundances of the H II regions as a function of the distance from the nucleus. Lines fitted to these points are also shown. Triangles represent oxygen, and squares represent nitrogen abundances. The open symbols correspond to the H II region to the W.

TABLE 4

H II REGIONS ABUNDANCES

PARAMETER	POSITION				
	46″.8 W	33″.3 E	43″.3 E	67″.5 E	81″ E
$12 + \log N^+/H^+$	7.91	7.97	7.95	7.82	7.58
$12 + \log S^+/H^+$	6.75	6.71	6.83	6.85	6.63
$12 + \log O^+/H^+$	8.64	8.65	8.73	8.66	8.53
$12 + \log O^{++}/H^+$	7.94	8.39	8.25	8.06	7.88
$12 + \log O/H$	8.77	8.84	8.85	8.76	8.62
$12 + \log N/H$	8.03	8.16	8.07	7.92	7.66
T[O III]	5760	5630	5520	6070	7260
T[O II]	7030	6940	6860	7250	8080
N_e (cm^{-3})	50	78	30	10	10

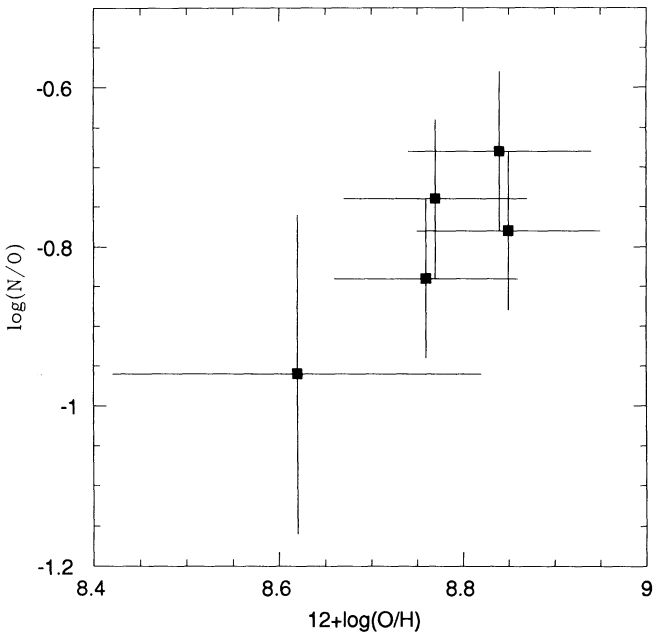

FIG. 14.—Logarithm of the ratio between the nitrogen and oxygen abundances as a function of the oxygen abundance.

these shifts are of the order of our uncertainties, we decided to keep our abundance values.

The observed gradients in O/H and N/H can be used to get extrapolated abundance values for the nucleus: $12 + \log (O/H) = 8.96 \pm 0.1$ ($\approx 1.1 \times$ solar) and $12 + \log (N/H) = 8.36 \pm 0.1$ ($\approx 2.4 \times$ solar).

4.4.2. *ENLR*

Using the above estimates, we assumed that the abundances in the nuclear region are solar for O and 2 times solar for N, in order to model the ENLR using CLOUDY. Based on previous works (Storchi-Bergmann & Pastoriza 1989, 1990) which suggest that N and S are overabundant in the nucleus of active galaxies, we set the S abundance, relative to the solar value, equal to that of N (also relative to the solar value). The other elements were kept at the solar value. In order to verify the effect of a varying abundance of N and S, we have also calculated models with solar and 3 times solar abundances for these elements. The other input parameters for the models were constant gas density $N = 300$ cm^{-3} (see Fig. 11), a typical AGN ionizing continuum (option "table AGN" in CLOUDY), and ionization parameter in the range $-3.5 \leq \log U \leq -2.0$. As we have found that the nuclear region is obscured, we have also calculated models including the presence of dust, with the chemical composition of the grains given by Cowie & Songaila (1986). The corresponding heavy element abundances were depleted from the abundance of the gas.

We show in Figure 15 the observed emission-line ratios [S II]/Hα, [N II]/Hα and [O III]/Hβ versus the reddening corrected [O II]/[O III] ratio for points within the ENLR, together with the model values. Although this region seems to extend to about 15″ from the nucleus, the emission-line ratios for the region between 9″ and 15″ present intermediate values between high-excitation and H II region ratios. The effect is more pronounced to the E. We conclude that the emission from this region is a mixture of contributions from the high-excitation

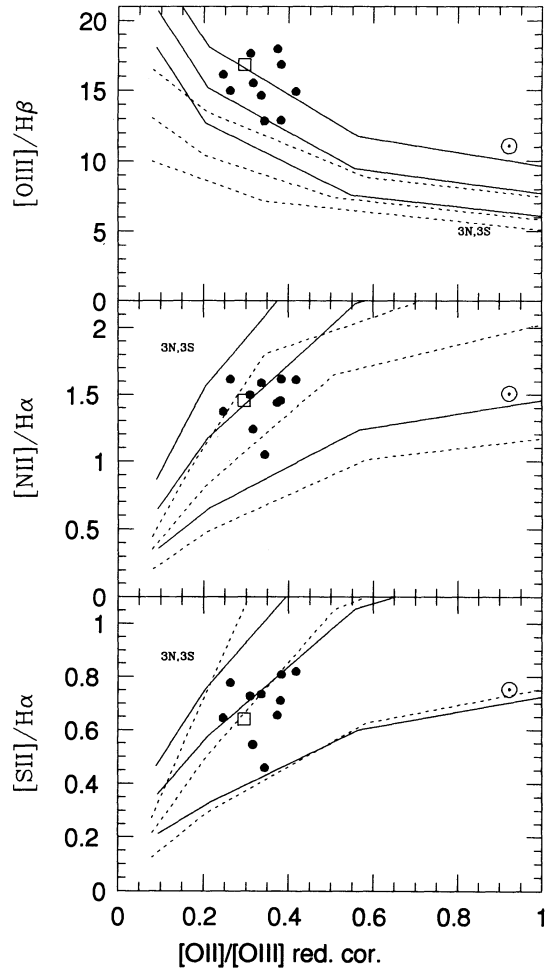

FIG. 15.—Comparison of the emission-line ratios of the high-excitation gas with photoionization models. The open squares represent the nucleus. Lines represent photoionization models for a gas density $n = 300$ cm^{-3} and ionization parameter in the range $-2.0 \leq \log U \leq -3.5$. Models with solar abundances are identified by the symbol ⊙. The models with nitrogen and sulphur abundance 3 times solar are indicated by 3N, 3S and the models with nitrogen and sulphur abundance 2 times solar are always the middle line. The ratio [O II]/[O III] was corrected for reddening using the measured Balmer decrement Hα/Hβ. The dashed lines are models without dust, and the solid lines are the models with dust.

gas and H II regions along the bar and decided to compare with the high-excitation models only the ratios within 9″ from the nucleus. From the figure it can be seen that [N II]/Hα and [S II]/Hα can be reproduced both by models with and without dust, for S and N abundances about 2 times solar in the models with dust, and for models with N and S 3 times solar for models without dust. This result agrees with that found by Storchi-Bergmann & Pastoriza (1989, 1990) for a large sample of Seyfert 2 galaxies and low-ionization nuclear emission-line regions (LINERs). These authors did not consider the presence of dust in their models. The present work shows that when dust is included, a smaller excess of nitrogen abundances relative to solar is required, and the general agreement between different line ratios is better. The [O III]/Hβ ratios from the ENLR of NGC 5643 are very high and do require the presence of dust to be reproduced. The values are somewhat higher than those predicted by the models with N and S 2 times solar—as

obtained from the other two diagrams and the H II region models.

In order to find a better agreement between the models and the observed emission-line ratio [O III]/Hβ, we tried to vary the O abundance of the gas, in the models, keeping the total abundance (gas + dust) of oxygen equal to the solar value. We obtained a slightly better agreement between the observed [O III]/Hβ ratio and the model values increasing the O abundance in the gas from 0.62 to 0.80 times the solar value, but the agreement was poorer for the ratios [N II]/Hα and [S II]/Hα. Then we realized that because of the small equivalent width of the Hβ emission, its flux is very sensitive to the underlying absorption—an underestimation of the correction by 10% is enough to bring the observed [O III]/Hβ ratio to the observed values with O solar and N and S 2 times solar abundances. We thus conclude that we have probably underestimated by about 10% the correction for underlying Hβ absorption in the high-excitation spectra and that the models which best reproduce the observations are the ones including dust, N and S abundances 2 times solar, and the other elements with solar abundance.

5. SUMMARY AND CONCLUSIONS

NGC 5643 seems to be another galaxy which fits into the "Unified Model" for Seyfert galaxies: the excitation map and distribution of emission-line ratios support previous suggestions that the ionizing continuum is collimated within a bicone; there is an increasing obscuration and increasing gas density toward a region $\approx 3''$ W from the nucleus, reinforcing the previous suggestion that the active nucleus is hidden there (calculations also show that on the assumption of isotropic nuclear emission, we are not seeing the nuclear light directly); we detect the presence of a blue continuum diluting the absorption lines in the inner 10″, which is probably due to nuclear scattered light; and the high-excitation emission and *IRAS* luminosity are consistent with the presence of a dusty torus obscuring the nuclear source and collimating its radiation in a cone. Our data also show that the cone axis is tilted such that we see excited gas in front of the bar to the E and behind the bar to the W.

We were able to obtain gas abundances for H II regions along the bar of NGC 5643 and found an increasing abundance toward the center, reaching O/H $\approx$ solar and N/H ≈ 2 times solar at the nucleus. The gradient in N/H is steeper than that of O/H and indicates both primary and secondary origin for nitrogen. Models for the ENLR gas can successfully reproduce the emission-line ratios if the presence of dust is taken into account and the abundances of N and O are those derived from extrapolation toward the nucleus of the H II region abundances, with the S abundance equal to that of N.

This work confirms previous results of an overabundance of nitrogen and sulphur found in the nucleus of ≈ 160 active galaxies from models of their NLR (Storchi-Bergmann & Pastoriza 1989, 1990), as we have shown that the abundances derived for the NLR agree with those obtained for the H II regions. But it is necessary to include the presence of dust, which makes the derived overabundance of N and S somewhat smaller (e.g., from 3 to 2 times solar in this case).

These enhanced metal abundances are not all that surprising. There is now considerable evidence for abundances of 2–10 times solar in the stars in the central regions of our Galaxy and others (Rich 1988; Arimoto & Yoshii 1986; Bica 1988; Bica, Arimoto, & Alloin 1988). The broad emission line regions in luminous QSOs also have high nitrogen abundances, ranging up to at least 10 times solar (Hamann & Ferland 1992, 1993; Baldwin et al. 1993). NGC 5643 and the other Seyferts studied by Storchi-Bergmann & Pastoriza (1989, 1990) are all massive galaxies in which the central stellar populations should have gone through much evolution, so that the gas found there should show evidence of the resultant nuclear processing.

This work was partially supported by the Brazilian institutions CNPq, FINEP, and FAPERGS. We are grateful to G. Ferland for making the CLOUDY photoionization code available to the general astronomical community. We also would like to thank F. Hamann and J. Shields for valuable suggestions about the dust composition and the referee R. Pogge for comments and suggestions which helped to improve the paper.

REFERENCES

Aller, L. H. 1987, in Spectroscopy of Astrophysical Plasmas, ed. A. Dalgarno & D. Layzer (Cambridge: Cambridge Univ. Press), p. 726
Alloin, D., Collin-Souffrin, S., Joly, M., & Vigroux, L. 1979, A&A, 78, 200
Antonucci, R. R. J. 1993, ARA&A, 31, 473
Antonucci, R. R. J., & Olszewski, E. W. 1985, AJ, 90, 2203
Arimoto, N., & Yoshii, Y. 1986, A&A, 164, 260
Baldwin, J. A., Ferland, G. J., Hamann, F., Carswell, R. F., Phillips, M. M., Wilkes, B., & Williams, R. E. 1993, in preparation
Bica, E. 1988, A&A, 195, 76
Bica, E., Arimoto, N., & Alloin, D. 1988, A&A, 202, 8
Boller, Th., Meurs, E. J. A., Brinkmann, W., Fink, H., Zimmermann, U., & Adorf, H.-M. 1992, A&A, 261, 57
Burstein, D., & Heiles, C. 1984, ApJS, 54, 33
Campbell, A. W., Terlevich, R., Melnick, J. 1986, MNRAS, 223, 811
Cowie, L. L., & Songaila, A. 1986, ARA&A, 24, 499
Dopita, M. A., & Evans, I. N. 1986, ApJ, 307, 431
Edelson, R. A., & Malkan, M. A. 1986, ApJ, 308, 59
Ferland, G. J. 1991, OSU Internal Rept. No. 91-01
Garnett, D. R. 1989, ApJ, 345, 282
———. 1990, ApJ, 363, 142
Grevesse, N. 1984, in Frontiers of Astronomy and Astrophysics, ed. R. Pallavicini (Florence: Italian Astron. Soc.), 71
Hamann, F., & Ferland, G. J. 1992, ApJ, 391, L53
———. 1993, ApJ, submitted
Kinney, A. L., Antonucci, R. R. J., Ward, M. J., Wilson, A. S., & Whittle, M. 1991, ApJ, 377, 100
McCall, M. L. 1984, MNRAS, 208, 253
McGaugh, S. S. 1991, ApJ, 380, 140
Morris, S., Ward, M., Whittle, M., Wilson, A. S., & Taylor, K. 1985, MNRAS, 216, 193
Mulchaey, J. S., et al. 1993, in preparation
Pagel, B. E. J., Edmunds, M. G., Blackwell, D. E., Chun, M. S., Smith, G. 1979, MNRAS, 189, 95
Phillips, M. M., Charles, P. A., & Baldwin, J. A. 1983, ApJ, 266, 485
Pier, E. A., & Krolik, J. H. 1992, ApJ, 401, 99
Pogge, R. W. 1988a, ApJ, 328, 519
———. 1988b, ApJ, 332, 702
Pogge, R. W., & De Robertis, M. M. 1993, ApJ, 404, 563
Reif, K., Mebold, U., Goss, W. M., van Woerden, H., & Siegman, B. 1982, ApJS, 50, 451
Rich, R. M. 1988, AJ, 95, 828
Roche, P. F., Aitken, D. K., Smith, C. H., & Ward, M. J. 1991, MNRAS, 248, 606
Sandage, A. 1978, AJ, 83, 904
Stone, R. P. S., & Baldwin, J. A. 1983, MNRAS, 204, 347
Storchi-Bergmann, T., & Bonatto, C. J. 1991, MNRAS, 250, 138
Storchi-Bergmann, T., Mulchaey, J. S., & Wilson, A. S. 1992, ApJ, 395, L73 (SBMW)
Storchi-Bergmann, T., & Pastoriza, M. G. 1989, ApJ, 347, 195
———. 1990, PASP, 102, 1359
Storchi-Bergmann, T., Wilson, A. S., & Baldwin, J. A. 1992, ApJ, 396, 45
Vila-Costas, M. B., & Edmunds, M. G. 1992, MNRAS, 259, 121
Wilson, A. S. 1992, in Physics of Active Galactic Nuclei, ed. S. J. Wagner & W. J. Duschl (Berlin: Springer-Verlag), 307